

Fluorite trace-element chemistry and its potential as an indicator mineral: Evaluation of LA-ICP-MS method



Mao Mao^{1,2,a}, George J. Simandl^{1,3}, Jody Spence³, and Daniel Marshall²

¹ British Columbia Geological Survey, Ministry of Energy and Mines, Victoria, BC, V8W 9N3

² Department of Earth Sciences, Simon Fraser University, Burnaby, BC, V5A 1S6

³ School of Earth and Ocean Sciences, University of Victoria, Victoria, BC, V8P 5C2

^a corresponding author: mao.mao13@outlook.com

Recommended citation: Mao, M., Simandl, G.J., Spence, J., and Marshall, D., 2015. Fluorite trace-element chemistry and its potential as an indicator mineral: Evaluation of LA-ICP-MS method. In: Simandl, G.J. and Neetz, M., (Eds.), Symposium on Strategic and Critical Materials Proceedings, November 13-14, 2015, Victoria, British Columbia. British Columbia Ministry of Energy and Mines, British Columbia Geological Survey Paper 2015-3, pp. 251-264.

1. Introduction

Fluorite (CaF_2) belongs to the isometric system, with a cubic, face-centred lattice. Fluorite commonly forms cubes or octahedrons, less commonly dodecahedrons and, rarely, tetrahedrons, trapezohedrons, trisoctahedrons, hexoctahedrons, and botryoidal forms. Fluorite is transparent to translucent, and has vitreous luster. It occurs in a variety of colours including purple, green, blue, or yellow, however it can also be colourless, and can exhibit colour zoning, (Staebler et al., 2006). Fluorite from many localities is fluorescent (Verbeek, 2006).

Fluorite density varies from 3.0-3.6 g/cm^3 , depending to a large extent on inclusions and impurities in the crystal lattice (Staebler et al., 2006), and its hardness is 4 on Mohs scale (Berry et al., 1983). Many single fluorite crystals display sector zoning, reflecting preferential substitution and incorporation of trace elements along successive crystal surfaces (Bosce and Rakovan, 2001). The Ca^{2+} ion in the fluorite crystal structure can be substituted by Li^+ , Na^+ , K^+ , Mg^{2+} , Mn^{2+} , $\text{Fe}^{2+,3+}$, Zn^{2+} , Sr^{2+} , Y^{3+} , Zr^{4+} , Ba^{2+} , lanthanides ions, Pb^{2+} , Th^{4+} , and U^{4+} ions (Bailey et al., 1974; Bill and Calas, 1978, Gagnon et al., 2003; Schwinn and Markl, 2005; Xu et al., 2012; Deng et al., 2014). Concentrations of these impurities do not exceed 1% (Deer, 1965) except in yttrifluorite $(\text{Ca,Y})\text{F}_{2-2.33}$ and cerfluorite $(\text{Ca,Ce})\text{F}_{2-2.33}$ (Sverdrup, 1968).

Fluorite occurs in a variety of rocks, as an accessory and as a gangue mineral in many metalliferous deposits and, in exceptional cases, as the main ore constituent of economic deposits (Simandl, 2009). Good examples of fluorite mines are Las Cuevas, Encantada-Buenavista (Mexico); St. Lawrence pluton-related veins and the Rock Candy Mine (Canada); El Hamman veins (Morocco) and LeBurg Montroc–Le Moulinal and Trebas deposits (France) as documented by Ruiz et al. (1980), Grogan and Montgomery (1975), González-Partida et al. (2003), Muñoz et al. (2005), and Fulton III and Miller (2006).

Fluorite also commonly occurs adjacent to or within carbonatites and alkaline complexes (Kogut et al., 1998;

Hagni, 1999; Alvin et al., 2004; Xu et al., 2004; Salvi and Williams-Jones, 2006); Mississippi Valley-type (MVT) Pb-Zn-F-Ba deposits; F-Ba-(Pb-Zn) veins (Grogan and Bradbury, 1967 and 1968; Baxter et al., 1973; Kesler et al., 1989; Cardellach et al., 2002; Levresse et al., 2006); hydrothermal Fe ($\pm\text{Au}$, $\pm\text{Cu}$) and rare earth element (REE) deposits (Borrok et al., 1998; Andrade et al., 1999; Fourie, 2000); precious metal concentrations (Hill et al., 2000); fluorite/metal-bearing skarns (Lu et al., 2003); Sn-polymetallic greissen-type deposits (Bettencourt et al., 2005); and zeolitic rocks and uranium deposits (Sheppard and Mumpton, 1984; Cunningham et al., 1998; Min et al., 2005).

Ore deposit studies that document the trace element distribution in fluorite are provided by Möller et al. (1976), Bau et al. (2003), Gagnon et al. (2003), Schwinn and Markl (2005), and Deng et al. (2014). The benchmark paper by Möller et al. (1976) identified variations in the chemical composition of fluorites according to their origin (sedimentary, hydrothermal, or pegmatitic).

Recently, Makin et al. (2014) compiled trace-element compositions of fluorite from MVT, fluorite-barite veins, peralkaline-related, and carbonatite-related deposits. They showed that fluorite from MVT and carbonatite deposits can be distinguished through trace element concentrations, and that the REE concentration of fluorite from veins is largely independent of the composition of the host rock. Based on the physical and chemical properties of fluorite, its association with a variety of deposit types, and previous studies, it is possible that fluorite can be used as a proximal indicator mineral to explore for a variety of deposit types. Unfortunately, the compilation by Makin et al. (2014) contained chemical analyses performed at different laboratories using different analytical techniques (including laser ablation-inductively coupled plasma mass spectrometry (LA-ICP-MS), electron microprobe, neutron activation, and ICP-MS), and precision and accuracy varied accordingly.

As an orientation survey, herein we present data from five deposits, with two samples from the Rock Candy deposit (British Columbia), and one sample from each of Kootenay

Florence (British Columbia), Eaglet (British Columbia), Eldor (Quebec), and Hastie quarry (Illinois) deposits (Table 1).

The main objectives of this study are to: 1) assess variations in chemical composition of fluorite in the samples and deposit types; 2) evaluate relations between analyses made using laser ablation-inductively coupled plasma mass spectrometry on individual grains [LA-ICP-MS(IG)], and those made using laser ablation-inductively coupled plasma mass spectrometry on fused beads [LA-ICP-MS(FB)] and X-ray fluorescence (XRF); 3) test the use of stoichiometric Ca content as an internal fluorite standard, such as has been done by Gagnon et al. (2003) and Schwinn and Markl, (2005); 4) select the elements that are commonly present in concentrations above the lower limit of detection of LA-ICP-MS and available for constructing discrimination diagrams; 5) consider if our results agree with the preliminary discrimination diagrams of Makin et al. (2014).

2. Laboratory methods

2.1. Sample preparation

Fluorite crystal fragments measuring 0.2-2.5 cm were broken from six fist-size rock samples. These fragments were crushed, and inclusion-free fluorite grains (0.5 to 3 mm) were selected under a binocular microscope. Grains from each inclusion-free fluorite concentrate were mounted and polished in epoxy pucks for in situ trace element analysis of individual grains by LA-ICP-MS(IG). The remaining material, approximately 25-35 fragments, was ground into powder using an agate mortar and fused into glass beads for bulk fused bead XRF and LA-ICP-MS(FB) analysis.

To determine the deviation of Ca composition of fluorite from the stoichiometry content, and to determine the accuracy of our LA-ICP-MS results, the Kootenay Florence (AHS-1) and the Rock Candy (RC-08-8) samples were duplicated to test the repeatability of fused-bead LA-ICP-MS and confirm the homogeneity of the powder.

2.2. In situ LA-ICP-MS(IG) analysis

LA-ICP-MS(IG) analyses of fluorite grains were performed on a Thermo X-Series II (X7) quadrupole ICP-MS at the School of Earth and Ocean Sciences, University of Victoria. For LA-ICP-MS(IG), a New Wave UP-213 was coupled to the X-Series II with Helium as the carrier gas.

Fluorite grains were analyzed with a 55 μm laser spot diameter, a pulse rate of 10 Hz, and measured fluence ranged from 7.69 to 12.55 $\text{J}\cdot\text{cm}^{-2}$. A pre-ablation warm-up of 5 seconds was used to avoid unstable laser energy at the beginning of each ablation. All spectra were recorded for 120 seconds including ~30 seconds gas blank before ablation started, 60 seconds during ablation, and ~30 seconds after ablation. At least 60 seconds of gas flushing occurred between analyses. The ICP-MS was optimized to maximize sensitivity and minimize oxide formation. Forward RF was 1400 watts. The dwell time was 10 ms for all elements.

A total of 114 analyses from 6 samples was obtained. For each sample, 12-42 data points were collected from different

grains, and most grains contain two random analyses for examining the trace element variations due to potential zoning.

The stoichiometric Ca content (51.33 wt.%) of fluorite was used as the internal standard for LA-ICP-MS calibration. NIST glass standards (611, 613, 615) were used for external calibration (Jochum et al., 2011). Each analysis session started with NIST glasses 615, 613, and 611, followed by the Rock Candy fluorite (potential secondary matrix-matched standard), and then six to seven unknowns, and then all four standards were repeated. During the data reduction, time-resolved count rates were carefully checked and any spectra with spikes, indicating possible inclusions, were excluded. The data reduction procedure for each element was: 1) selection of the time intervals for the background and signal region of each spectrum; 2) calculation of the mean CPS (counts per second) of these intervals; 3) background correction of the signal CPS; 4) external and internal standard normalizations; 5) drift correction using a linear drifting factor determined from repeat analyses of NIST 611; and 6) calibration using sensitivities for each element determined from the initial analyses of NIST 615, 613 and 611 in each load to achieve the concentration value of each element.

Thirty-nine trace elements were analyzed by LA-ICP-MS(IG) for reconnaissance. The experimental precision was determined by repeat analyses of NIST glasses 613 and 615. Based on NIST 613, the 2σ precision for elements with concentrations ranging from dozens to several hundred ppm is <10% for Mg, Mn, Rb, Sr, Y, Ba, lanthanide, W, Pb, Th and U; and from 10% to 15% for Fe. For NIST 615, which contains lower concentrations of all elements than NIST 613, the precision is 10-15% for Rb, Nb, Ba, Pr, Eu, Tb, Ho, Tm, Lu, W, Pb, and Th; between 15-20% for Mg, Zr, Sm, Er, Yb, and U; from 20% to 25% for Dy; and >25% for other elements.

Due to instrument drifting, the limit of detection (LOD) was determined for each element per session using the following:

$$\text{LOD} = \frac{3 \times (\text{STDev background signal})}{\text{Sensitivity (per analyte element, per session)}}$$

where 'STDev background signal' is the standard deviation of the signal for a given element collected before ablation for each sample (gas blank), and 'Sensitivity' is the calibrated sensitivity determined from NIST 615, 613 and 611 in each session.

The detection limits are typically <20 ppm for Fe; <15 ppm for Sr; <5 ppm for Mg; <3 ppm for Mn and Y; <2 ppm for Ba; <1 ppm for Rb, Ce, Nd, and Pb; <0.5 ppm for La, Pr, Sm, Gd, Dy, Th, and U; <0.2 ppm for Zr, Nb, Mo, Eu, Tb, Ho, Er, Tm, Yb, Lu, and W.

2.3. Fused bead XRF and LA-ICP-MS(FB) analysis

Milled samples (Table 2) were shipped to Bureau Veritas Mineral Laboratories (ACME) in Perth, Australia for bulk XRF and LA-ICP-MS(FB) analysis. An aliquot of sample was weighed and intimately mixed with $\text{LiBO}_2/\text{Li}_2\text{B}_4\text{O}_7$ flux into a platinum crucible and fused in an electric furnace. The

Table 1. Summary of the fluorite-bearing deposits sampled for this study.

Deposit name	Deposit type	Main host rock	Key information	Mineral assemblage
Eldor, QC	Carbonatite-related REE±fluorite±apatite	Carbonatite complex (1.88-1.87 Ga, U-Pb); Pcl and columbite in the 2nd stage carbonatite; REE±fl in the 3rd stage carbonatite. (Gagnon et al., 2012).	At the contact of SC (Proterozoic metasedimentary rocks and amphibolites) and Gerido (Le Moyne and Doublet groups, and Eldor carbonatite) zones (Gagnon et al., 2012).	3rd stage (A zone) contains 1.5-3+% TREO (mnz) +fl+breunnerite in Fe-dol matrix. Accessory minerals are ap, py, sp, mag, xtm, qz, Nb-bearing rt, nioboaeschynite, ferrocolumbite and ilm (Wright et al., 1998; Gagnon et al., 2012).
Eaglet, BC	Fluorite-barite vein/porphyry Mo granite-syenite related	Early Mississippian granitic orthogneiss (375-335 Ma, U-Pb zircon; Mortensen et al., 1987) intruded by dikes and pods of aplite, pegmatite, lamprophyre and feldspar-porphyry dikes, adjacent to contact with the Neoproterozoic biotite-garnet metapelite (Pell, 1992).	Fl veinlets/veins/pod disseminated on mol in the proximity of the fl mineralization but not overlapping (Hora et al., 2008).	Qz, mol, fl, carbonate minerals, clt, prismatic REE-bearing carbonates, gn, sp, py, gp, aln, pcl (Pell, 1992; Hora et al., 2008).
Rock Candy, BC	Fluorite-barite vein	Tertiary andesitic volcanic rocks adjacent to Coryell syenite intrusion. Subparallel veins from a few cm to 10 m wide and breccia in a silicified fracture zone (MINFILE BC, 082ESE070).	Breccia and composite veins with multiple generations of green and purple fl are exposed in a trench, containing fragments of severely-altered country rock (Pell, 1992).	Fl, brt, chalcedony, kln, py, qz, and cal (Pell, 1992; Mauthner and Melanson, 2006).
Kootenay Florence, BC	Sedimentary-related Ag-Pb-Zn/Polymetallic Ag-Pb-Zn vein	1) veins and replacements along contact with limestone and overlaying schist; 2) fissure veins in contact with quartz and sheared greenstone (MINFILE BC, 082FNE016).	Sample cavity at the No. 7 level at the contact between vein and limestones (Fyles, 1967).	Ore minerals: coarsely crystalline gn, sp, py, pcl, and ccp. Gangue minerals: fl, qz and cal (Pell, 1992; Mauthner and Melanson, 2006).
Hastie Quarry, IL	MVT	In bedded replacement zones parallel to Mississippian host rocks, which are mainly oolitic or fossiliferous limestones underlying a sandstone unit (Pelch et al., 2015). Age of mineralization is 272 ±17 Ma (fluorite, Sm-Nd; Chesley et al., 1994).	Steeply dipping faults and fractures are spatially associated with the deposits and may have acted as feeders for mineralizing fluids (Pelch et al., 2015).	Fluorite occurs in hydrothermal Stage II and III with sp, gn, qz, and ccp. Gangue minerals: brt, qz, and cal (Richardson and Pinckney, 1984; Pelch et al., 2015).

Table 2. Summary of fluorite samples and analyses.

Sample Name	Deposit/Locality Name	Fluorite Color	No. of Analyses LA-ICPMS(IG)	No. of Analyses LA-ICPMS(FB)
ELDOR2	Eldor, QC	Purple	23	1
EAGLET9	Eaglet, BC	Light Purple	12	1
RC-08-5P	Rock Candy, BC	Purple	12	1
RC-08-8	Rock Candy, BC	Green	42	2
AHS-1	Kootenay Florence, BC	Pale green	13	2
HQ-3-12S-9EY	Hastie quarry, IL	Yellow	12	1

melt was kept at constant temperature, and poured into a glass bead. The beads were analyzed using XRF Spectroscopy, for Ca, F, and Ba, and for LA-ICP-MS(FB) using a New Wave NWR193 coupled to an Agilent 7700 for 59 trace elements (Bureau Veritas Mineral Laboratories, 2015). Each fused bead of fluorite was ablated for 60 seconds with a laser spot size of 150 μm in diameter, a pulse rate of 20 Hz, and measured fluence of minimum 5 J/cm^2 . Data reduction was performed using the LIMS software (Sorby Minerals) and a proprietary internal calibration and standardization process, of Bureau Veritas Mineral Laboratories. No external standard was used.

3. Results

In total, 114 analyses from 51 individual fluorite grains were performed using LA-ICP-MS(IG). Eight equivalent samples in form fused beads were analyzed using XRF and LA-ICP-MS(FB) for major and minor elements (Table 2).

3.1. Results of XRF and LA-ICP-MS(FB)

The XRF results show that the Ca contents from 8 analyses of different fluorites range between 51.0% and 51.3% (Table 3). The F content of the samples ranges from 48.4% to 48.8% (Table 3), and the Ba concentrations are consistently below detection limit (0.01%).

The LA-ICP-MS(FB) results (Table 3) show that Sr contents are from 95.6 to 4,880 ppm; Y contents are from 15 to 337 ppm; Zn contents are from 50 to 175 ppm; Cu content varies from below the detection limit to 48 ppm; lanthanide contents are from 3.5 to 299 ppm. Elements with concentrations between 1 ppm and above the limit of detection are Be, Co, As, Rb, Nb, Mo, Ag, Cd, Sn, Te, Hf, Ta, W, Bi, and U. Elements that are almost always consistently below the detection limit are Sc, Ga, Ge, In, Se, Cs, Re, and Tl.

3.2. Results of LA-ICP-MS(IG)

Strontium concentrations across all analyzed fluorite have large variations, from 47 to 3,526 ppm. Fluorite from the Hastie Quarry (HQ-3-12s-9EY) has the lowest Sr contents (47-103 ppm). The range of Sr concentrations in Kootenay Florence (AHS-1) samples overlap with those from Hastie Quarry, but are slightly higher (83 to 142 ppm). Fluorite from Eaglet (Eaglet9) has the highest Sr contents (2,679-3,526 ppm). Fluorite from Eldor (Eldor2) has the second highest Sr contents (920-1,112 ppm). Fluorite from Rock Candy (RC-08-8 and RC-08-5p) has a variation in Sr content from 177 to 654 ppm (Table 4).

Yttrium contents range from 4 to 1,448 ppm. Hastie Quarry samples have consistently low Y concentrations, from 9 to 13 ppm. Kootenay Florence samples have a range from 6 to 31 ppm Y. The Y concentrations in Eaglet samples vary from 44 to 60 ppm; those from Eldor vary from 153 to 220 ppm. The analyses of Y concentrations from Rock Candy yield the widest variation, from 4 to 1,448 ppm (Table 4).

Total REE content is restricted to the lanthanides. The light REE (LREE) analyses include La, Ce, Pr, Nd, Sm, Eu, and Gd (it does not include Sc). The heavy REE (HREE) analyses

include Tb, Dy, Ho, Er, Tm, Yb, and Lu (it does not include Y). Contents of the sum of the lanthanides of all analyzed fluorite range from 2 to 831 ppm. The lowest ΣREE contents are from Hastie Quarry (2.26-2.59 ppm). Fluorite from Kootenay Florence is also low in the ΣREE contents (4.43-6.49 ppm). The sums of LREE (ΣLREE) contents in fluorite from Hastie Quarry are the lowest, from 1.03 to 1.43 ppm. Kootenay Florence has the second lowest ΣLREE , ranging from 2.69 to 6.00 ppm. For the sum of HREE (ΣHREE), Kootenay Florence has the lowest contents from 0.72 to 1.59 ppm, and the Hastie Quarry samples are also low in ΣHREE ranging from 1.01 to 1.25 ppm. Fluorite from Rock Candy has the largest variation in ΣREE contents ranging from 10 to 831 ppm; the variations of ΣLREE and ΣHREE are also the largest, ranging from 9 to 534 ppm and from 2 to 296 ppm, respectively (Table 4).

Iron contents in the fluorite samples display a relatively limited range, from 104 to 184 ppm (Table 4), and there are no distinct differences between any of the samples. Manganese contents of most samples (92 analyses) are below detection limit (1-3 ppm typically), except for some grains from the Rock Candy and Eaglet deposits. Manganese is detectable in almost all grains from Eaglet, with contents of 3-5 ppm. Magnesium, Sc, Ti, V, Cu, Zn, Zr, Nb, Mo, Rb, Ba, W, Th, and U are rarely present at concentrations above the detection limits (Table 4).

4. Discussion

The calculated XRF average Ca content of analyzed fluorite samples is 51.18%, and the variation of Ca contents through all fluorite samples is 0.2%. This is very similar to the stoichiometric Ca content of fluorite (51.33%), which indicates that it is appropriate to use the stoichiometric Ca content (51.33%) as the internal standard for LA-ICP-MS data reduction and to construct traditional Tb/Ca–Tb/La discrimination diagrams that were popularized by Möller (1976).

4.1. Elements for constructing discrimination diagrams

Elements that may be suitable for constructing discrimination diagrams can be assessed based on the concentrations of individual elements and the relationships between elements in concentrations above detection limits.

4.1.1. Concentrations of individual elements

Based on our results, Fe, Sr, Y, and the lanthanides are consistently in concentrations above LA-ICP-MS(IG) detection limits. Strontium contents have relatively restricted, deposit-specific concentration ranges (Fig. 1a), with relatively low (~ 100 ppm) values from Kootenay Florence and Hastie quarry, and distinctly higher values from Rock Candy (~ 500 ppm), Eldor, and Eaglet fluorite (≥ 900 ppm). The Y contents of samples from these deposits show a comparable pattern to Sr. Both samples from Rock Candy show large variations, beyond those of all other samples (Fig. 1b). Based on similarities of elemental concentrations and distributions, the lanthanides can be divided into four groups: 1) La, Ce, Pr, Nd; 2) Sm, Eu; 3) Gd, Tb, Dy, Ho, Er; and 4) Tm, Yb, Lu. Hastie Quarry fluorite

Table 4a. Trace-element contents (ppm) of fluorite grains from Rock Candy and Kootenay Florence. M.D.L.: Minimum Detection Limit. BDL: Below detection limit. * Total REE content is restricted to lanthanides.

Quartile	RC-08-8, 42 analyses					RC-08-5P, 12 analyses					AHS-1, 13 analyses					
	Min	1st quartile	Median	3rd quartile	Max	Min	1st quartile	Median	3rd quartile	Max	Min	1st quartile	Median	3rd quartile	Max	M.D.L.
Mg	BDL	BDL	BDL	BDL	0.58	BDL	BDL	BDL	BDL	0.73	BDL	BDL	BDL	BDL	1.02	0.18
Sc	BDL	BDL	BDL	BDL	BDL	BDL	BDL	BDL	BDL	0.09	BDL	BDL	BDL	BDL	BDL	0.04
Ti	BDL	0.09	0.12	0.12	0.12	BDL	0.06	0.09	0.12	0.12	BDL	0.05	0.07	0.12	0.12	0.02
V	BDL	BDL	BDL	BDL	BDL	BDL	BDL	BDL	BDL	BDL	BDL	BDL	BDL	BDL	BDL	0.01
Mn	BDL	BDL	BDL	BDL	BDL	BDL	0.96	1.52	4.01	6.47	BDL	BDL	BDL	BDL	BDL	0.09
Fe	127.31	145.94	148.76	148.76	177.00	145.50	151.08	155.15	166.63	177.76	138.37	148.05	149.22	152.25	164.27	1.40
Cu	BDL	BDL	BDL	BDL	0.24	BDL	BDL	BDL	BDL	BDL	BDL	BDL	BDL	BDL	0.57	0.05
Zn	BDL	BDL	BDL	BDL	BDL	BDL	BDL	BDL	BDL	BDL	BDL	BDL	BDL	BDL	0.09	0.06
Rb	BDL	BDL	BDL	BDL	BDL	BDL	BDL	BDL	BDL	0.12	BDL	BDL	BDL	BDL	0.02	0.01
Sr	177.86	375.02	391.25	490.16	654.74	416.93	485.16	526.61	625.86	643.73	83.67	92.69	96.75	127.03	142.18	0.15
Y	3.97	14.77	28.55	33.37	42.00	24.53	76.99	183.32	236.32	1448.55	6.04	13.62	15.98	19.91	31.46	0.05
Zr	BDL	BDL	BDL	BDL	BDL	BDL	BDL	BDL	0.03	0.05	BDL	BDL	BDL	BDL	BDL	0.01
Nb	BDL	BDL	BDL	BDL	BDL	BDL	BDL	BDL	0.02	0.02	BDL	BDL	BDL	BDL	BDL	0.01
Mo	BDL	BDL	BDL	BDL	0.03	BDL	BDL	BDL	0.02	0.04	BDL	BDL	BDL	BDL	BDL	0.01
Ba	BDL	BDL	BDL	0.07	0.14	0.35	0.51	0.57	0.77	1.02	BDL	BDL	BDL	BDL	0.51	0.01
La	BDL	2.60	3.32	7.50	11.30	2.42	8.01	11.33	15.89	52.02	BDL	0.36	0.78	0.88	1.13	0.01
Ce	BDL	5.82	6.98	12.14	19.80	6.14	18.23	25.11	36.14	123.23	BDL	0.38	0.78	1.04	1.37	0.01
Pr	BDL	BDL	1.00	1.22	2.39	0.89	2.65	3.62	5.36	20.98	BDL	0.08	0.16	0.21	0.23	0.01
Nd	BDL	2.52	5.77	6.69	11.09	4.10	11.62	18.00	26.59	134.55	BDL	0.69	0.94	1.22	1.60	0.03
Sm	0.07	0.07	1.50	1.87	2.32	2.02	4.88	8.52	12.83	65.84	0.07	0.21	0.30	0.35	0.59	0.05
Eu	BDL	BDL	0.55	1.05	1.30	1.02	2.60	4.32	6.09	29.64	BDL	BDL	0.08	0.12	0.22	0.02
Gd	BDL	BDL	2.10	2.80	3.37	2.71	7.14	13.73	19.02	108.65	BDL	0.38	0.63	0.80	1.08	0.19
Tb	0.02	0.02	0.18	0.36	0.45	0.61	1.47	2.95	3.96	19.62	0.02	0.05	0.09	0.11	0.15	0.01
Dy	0.10	0.10	1.37	2.45	3.02	4.68	11.60	22.45	29.95	135.73	0.10	0.36	0.60	0.75	1.08	0.02
Ho	BDL	BDL	0.27	0.49	0.71	0.83	2.22	4.36	5.78	26.38	BDL	0.08	0.11	0.17	0.24	0.01
Er	0.05	0.05	0.76	1.51	2.06	2.61	6.79	12.37	16.40	67.79	0.05	0.17	0.23	0.36	0.67	0.02
Tm	BDL	BDL	BDL	0.16	0.25	0.38	0.96	1.62	2.04	6.93	BDL	BDL	BDL	0.02	0.03	0.01
Yb	BDL	BDL	0.80	1.32	1.79	2.65	6.41	9.73	12.84	36.01	BDL	0.04	0.07	0.11	0.25	0.01
Lu	BDL	BDL	0.05	0.19	0.28	0.36	0.80	1.17	1.52	3.98	BDL	BDL	BDL	BDL	0.02	0.01
W	BDL	BDL	BDL	BDL	BDL	BDL	0.04	0.05	0.06	0.27	BDL	BDL	BDL	BDL	0.10	0.01
Pb	BDL	BDL	BDL	BDL	BDL	BDL	BDL	BDL	BDL	BDL	BDL	BDL	BDL	BDL	0.05	0.01
Th	BDL	BDL	BDL	0.02	0.15	BDL	BDL	BDL	BDL	0.97	BDL	BDL	0.12	0.22	0.29	0.01
U	BDL	BDL	BDL	0.01	0.43	BDL	BDL	0.02	0.07	0.10	BDL	BDL	BDL	BDL	BDL	0.01
ΣLREE	8.38	18.77	21.26	31.58	43.16	16.58	48.33	70.90	101.74	426.25	1.89	2.76	3.43	4.26	4.99	--
ΣHREE	2.99	5.35	8.36	9.91	18.78	14.83	37.39	69.10	91.44	405.10	1.10	1.41	1.68	2.17	2.67	--
ΣREE*	10.39	28.69	32.71	43.02	48.92	31.41	83.76	141.71	193.17	831.35	4.43	4.45	4.53	5.28	6.49	--

Table 4b. Trace-element contents (ppm) of fluorite grains from Eaglet, Eldor, and Hastie Quarry. M.D.L.: Minimum Detection Limit. BDL: Below detection limit. * Total REE content is restricted to lanthanides.

Quartile	Eaglet ⁹ , 12 analyses				Eldor ² , 23 analyses				HQ-3-12s-9EY, 12 analyses				M.D.L.			
	Min	1st quartile	Median	3rd quartile	Max	Min	1st quartile	Median	3rd quartile	Max	Min	1st quartile		Median	3rd quartile	Max
Mg	BDL	BDL	1.21	2.50	3.29	BDL	BDL	BDL	2.58	23.21	BDL	BDL	1.61	2.05	5.93	0.18
Sc	BDL	BDL	BDL	BDL	BDL	BDL	BDL	BDL	BDL	BDL	BDL	BDL	BDL	BDL	BDL	0.04
Ti	0.04	0.08	0.12	0.12	0.13	BDL	0.12	0.12	0.12	0.17	0.03	0.12	0.12	0.12	0.50	0.02
V	BDL	BDL	BDL	BDL	0.39	BDL	BDL	BDL	BDL	2.62	BDL	BDL	BDL	BDL	BDL	0.01
Mn	BDL	3.94	4.36	4.95	5.27	BDL	BDL	BDL	BDL	0.86	BDL	BDL	BDL	BDL	BDL	0.09
Fe	119.77	130.86	137.93	140.82	184.31	104.44	115.23	127.80	131.27	159.26	133.80	143.88	147.29	149.68	157.78	1.40
Cu	BDL	BDL	BDL	BDL	0.07	BDL	BDL	BDL	BDL	9.13	BDL	BDL	BDL	BDL	0.22	0.05
Zn	BDL	BDL	BDL	BDL	BDL	BDL	BDL	BDL	BDL	2.81	BDL	BDL	BDL	BDL	BDL	0.06
Rb	BDL	BDL	BDL	BDL	BDL	BDL	BDL	BDL	BDL	BDL	BDL	BDL	BDL	BDL	0.04	0.01
Sr	2679.63	2735.74	3005.05	3115.71	3526.60	920.25	975.75	1001.14	1020.51	1112.04	47.01	82.20	85.50	91.18	103.81	0.15
Y	44.58	49.37	51.58	55.64	60.44	153.27	158.62	173.87	184.12	220.27	9.80	11.33	12.20	12.87	13.12	0.05
Zr	BDL	BDL	BDL	BDL	BDL	BDL	BDL	BDL	BDL	0.04	BDL	BDL	BDL	BDL	BDL	0.01
Nb	BDL	BDL	BDL	BDL	BDL	BDL	BDL	BDL	BDL	0.05	BDL	BDL	BDL	BDL	BDL	0.01
Mo	BDL	BDL	BDL	0.02	0.06	BDL	BDL	BDL	BDL	0.02	BDL	BDL	BDL	BDL	BDL	0.01
Ba	BDL	BDL	BDL	0.03	0.05	BDL	BDL	BDL	0.02	1.06	BDL	0.13	0.14	0.16	0.17	0.01
La	BDL	1.13	1.23	1.44	2.86	BDL	BDL	0.10	0.18	0.50	BDL	BDL	BDL	BDL	BDL	0.01
Ce	BDL	3.74	3.98	6.28	11.68	BDL	0.41	0.51	0.62	1.30	BDL	0.03	0.04	0.04	0.04	0.01
Pr	BDL	0.78	0.91	1.68	2.44	BDL	BDL	0.10	0.13	0.20	BDL	0.02	0.02	0.02	0.02	0.01
Nd	BDL	5.59	6.07	11.67	14.36	BDL	0.75	0.86	0.99	1.26	BDL	0.23	0.26	0.28	0.29	0.03
Sm	0.07	2.24	2.40	3.62	4.18	0.07	0.66	0.74	0.79	0.90	0.07	0.22	0.23	0.25	0.26	0.05
Eu	BDL	0.74	0.85	1.31	1.61	BDL	0.46	0.49	0.51	0.57	BDL	0.08	0.09	0.10	0.12	0.02
Gd	BDL	3.44	3.72	4.56	5.17	BDL	2.30	2.42	2.57	2.95	BDL	0.58	0.65	0.68	0.74	0.19
Tb	0.02	0.31	0.43	0.56	0.65	0.02	0.47	0.49	0.54	0.62	0.02	0.08	0.09	0.09	0.10	0.01
Dy	0.10	2.56	2.69	3.12	3.55	0.10	3.83	3.95	4.30	4.97	0.10	0.51	0.56	0.57	0.61	0.02
Ho	BDL	0.50	0.55	0.60	0.68	BDL	0.87	0.89	0.94	1.11	BDL	0.09	0.11	0.11	0.12	0.01
Er	0.05	1.40	1.49	1.58	1.78	0.05	2.56	2.68	2.82	3.31	0.05	0.22	0.25	0.26	0.27	0.02
Tm	BDL	0.11	0.17	0.18	0.20	BDL	0.29	0.30	0.33	0.38	BDL	0.02	0.02	0.03	0.03	0.01
Yb	BDL	1.00	1.08	1.19	1.28	BDL	1.88	2.01	2.10	2.33	BDL	0.08	0.10	0.11	0.12	0.01
Lu	BDL	0.13	0.14	0.15	0.17	BDL	0.24	0.26	0.28	0.34	BDL	BDL	BDL	BDL	0.02	0.01
W	BDL	0.07	0.10	0.13	0.17	BDL	BDL	0.04	0.07	0.11	BDL	0.02	0.02	0.03	0.03	0.01
Pb	BDL	BDL	BDL	0.03	0.04	BDL	BDL	BDL	0.02	1.53	BDL	BDL	BDL	BDL	0.02	0.01
Th	BDL	BDL	BDL	BDL	BDL	BDL	BDL	BDL	BDL	0.26	BDL	0.24	0.28	0.31	0.37	0.01
U	0.00	0.00	0.02	0.03	0.04	BDL	BDL	BDL	BDL	BDL	BDL	BDL	BDL	BDL	BDL	0.01
ΣLREE	12.54	14.87	17.46	30.42	36.63	2.33	2.66	2.97	3.31	4.59	0.54	0.63	0.64	0.69	0.69	--
ΣHREE	9.06	10.13	10.20	12.40	13.08	11.68	12.63	13.02	14.10	16.00	1.64	1.75	1.84	1.88	1.90	--
ΣREE	21.59	24.95	25.22	45.80	49.05	14.00	15.54	16.62	17.21	19.16	2.26	2.39	2.47	2.53	2.59	--

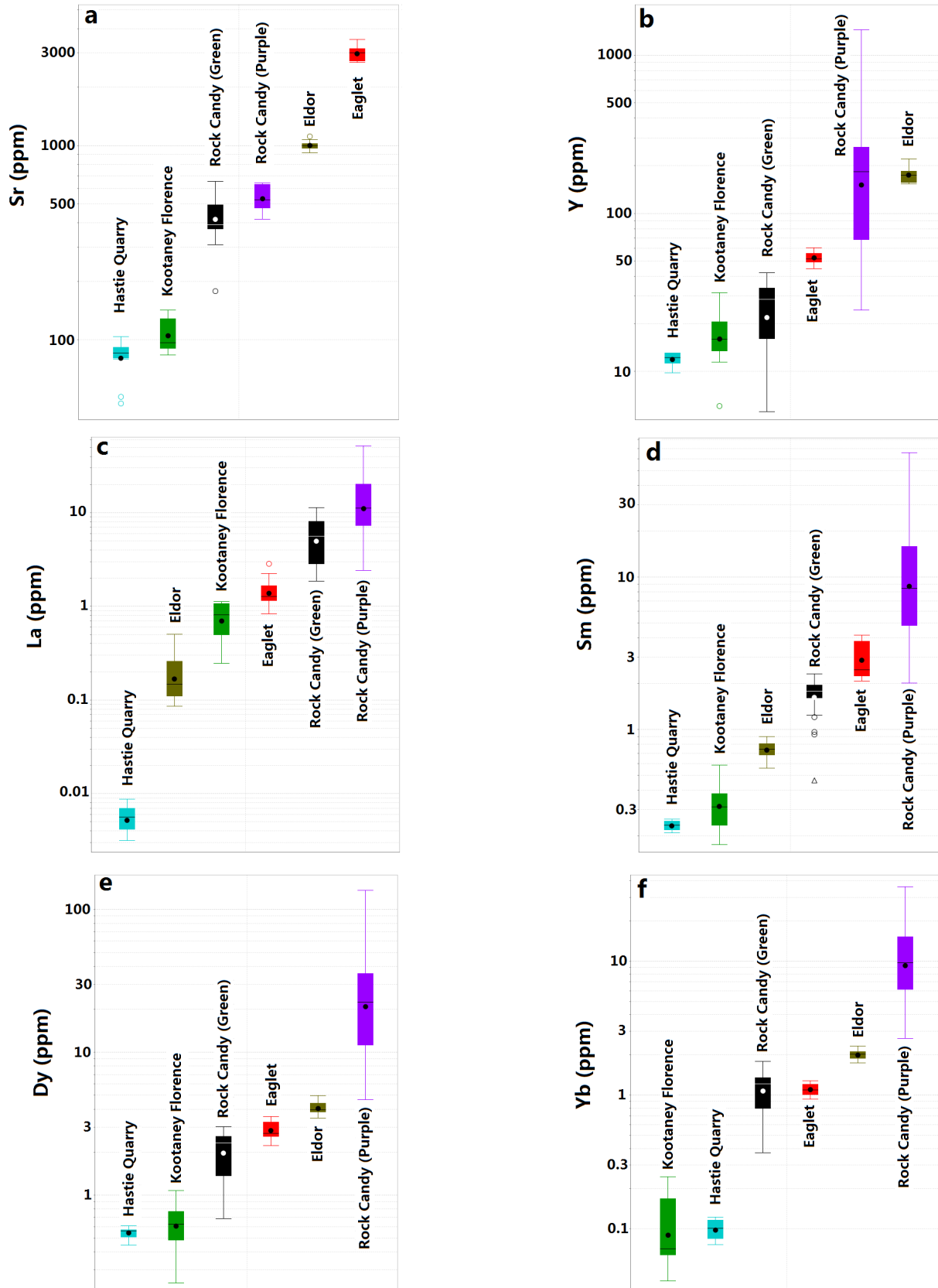


Fig. 1. Box plots of selected element contents of fluorite for each group: a) Sr; b) Y; c) La; d) Sm; e) Dy; f) Yb. Line: median value; solid dot: mean value; box: interquartile range (25th-75th percentile); open circle (outlier): further than $[1.5 \times (75^{\text{th}} \text{ percentile} - 25^{\text{th}} \text{ percentile})]$; open triangle (outlier): further than $[3 \times (75^{\text{th}} \text{ percentile} - 25^{\text{th}} \text{ percentile})]$; whiskers: extreme values that are not outliers.

contains the lowest La contents (<0.01 ppm), the Rock Candy fluorite has the highest La contents (2-14 ppm), and in the other three deposits La contents overlap (Fig. 1c). From La to Nd of the lanthanides, the compositions of the Eaglet samples rise to those of Rock Candy samples, and the contents of Kootenay Florence and Eldor samples become increasingly close to each other. Kootenay Florence and Hastie Quarry have the lowest Sm (~0.1-0.6 ppm) and Eu contents, whereas Eldor, Rock Candy (Green) and Eaglet all have higher Sm and Eu contents, with small ranges. The Rock Candy sample (purple) shows the highest Sm (~2-33 ppm) and Eu contents and the broadest variation (Fig. 1d). Element content patterns for Gd, Tb, Dy, Ho, and Er are almost identical, thus Dy is used as a representative for this group. Dysprosium contents range from ~0.2-1 ppm and are the lowest for Kootenay Florence and Hastie Quarry (Fig. 1e). Dysprosium contents of Rock Candy (Green) samples lie between, and partially overlap, Kootenay Florence and Eaglet samples (Fig. 1e). Eldor samples yield higher concentrations, but again, the Rock Candy sample (purple) has the highest Dy contents with the most variation (Fig. 1e). Ytterbium, together with Tm and Lu, is low in fluorite from Hastie Quarry and Kootenay Florence (around 0.1 ppm), but high in fluorite from other deposits. The Yb range is particularly well restricted in Eaglet and Eldor samples (Fig. 1f).

These results suggest that Sr, Y, and the lanthanides are strong contributors for discriminating the different deposits and rock types in simple X-Y plots. For example, plotting Nd vs. Sr concentrations (Fig. 2) displays distinct clustering for each of the different deposits. The fluorite from Rock Candy (fluorite-barite veins) and Eaglet contains higher Nd (generally greater than 4 ppm), and the fluorite from Hastie Quarry and Kootenay Florence (sedimentary-related deposits) have low Sr and Nd concentrations. The Eldor fluorite samples (carbonatite-related deposit) form a distinct group, with elevated Sr concentrations and Nd concentrations below 4 ppm.

Iron concentrations are similarly variable in all samples, and range consistently from 104 to 184 ppm, precluding its use for

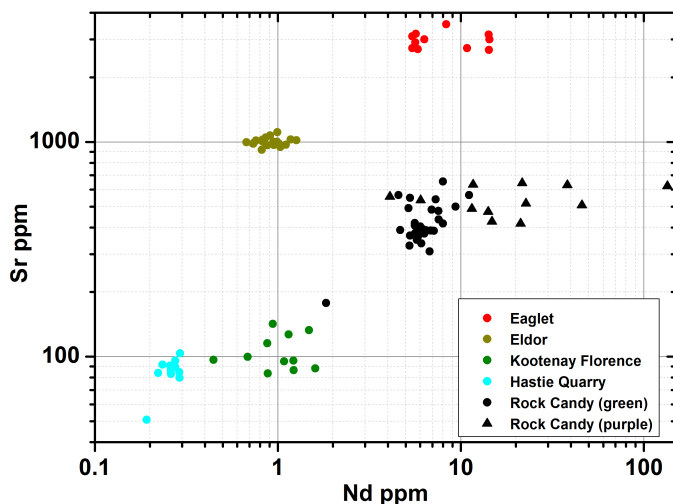


Fig. 2. Nd vs. Sr scatterplot for fluorite from different deposits.

discriminating deposit and rock types. On the other hand, many elements such as Mn, Ba, and Th are detectable, and they may be diagnostic for specific deposit types. The project requires additional data from different samples and deposits to develop comprehensive discrimination methods; this work is ongoing.

4.1.2. Relationships between elements

Fluorite from the MVT deposit (Hastie Quarry) and a limestone-related Ag-Pb-Zn mine (Kootenay Florence) have lower concentrations of trace elements, especially Sr, Y, Sm, Eu, Gd, and HREE relative to higher temperature deposits (Figs. 1-3; Table 4). From Y-Yb (Fig. 3) and Tb/La-Tb/Ca plots (Fig. 4), the concentrations of impurities in fluorite can separate the sedimentary-related deposits from the other deposits.

Eaglet and Rock Candy fluorite lie in the hydrothermal field of the Tb/Ca vs. Tb/La diagram (Fig. 4). Rock Candy fluorite shows wide variation in concentrations of Nd (Fig. 2), Y, Yb (Fig. 3), Tb, and Tb/La ratio (Fig. 4). The variation of Tb/Ca and Tb/La from sample RC-08-8 (green Rock Candy) probably reflects the REE fractionation during mineralization (Möller, 1976). The trend from sample RC-08-5P (purple Rock Candy) is distinct from both the fractionation trend during mineralization and the remobilization trend (Fig. 4), and shows a progressive increase in Tb relative to Tb/La fractionation. We are unsure what causes this trend, but speculate that it might record a magmatic overprint. Although fluorite from the Rock Candy deposit is associated with barite, its Ba content remains below detection limits. Fluorite from the Eaglet deposit shows little concentration variations for Sr, Nd (Fig. 2), Y, Yb (Fig. 3), Tb, and Tb/La (Fig. 4). The high Sr concentration in Eaglet fluorite coincides with co-existing celestite in mineralized zones (Hora et al., 2008).

Fluorite from Eldor, a carbonatite-related deposit, plots in

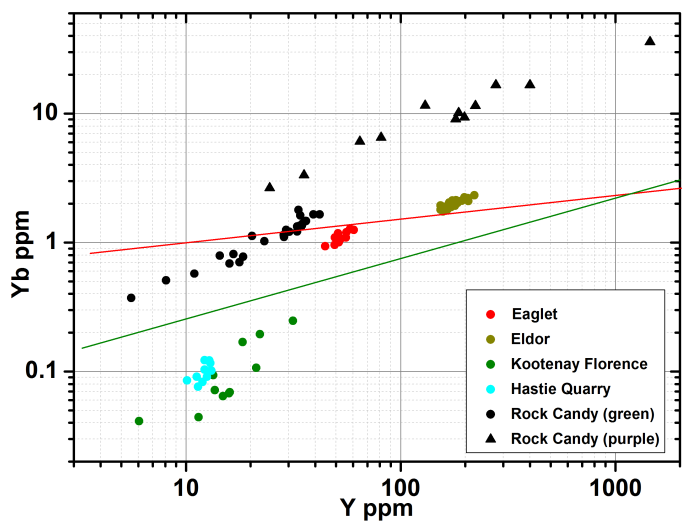


Fig. 3. Y vs. Yb scatterplot for fluorite from different deposits. The solid red line defined by Makin et al. (2014) is the boundary between MVT-related fluorite and carbonatite-related fluorite. The solid green line separates the fluorite from sedimentary-related deposits and other deposits.

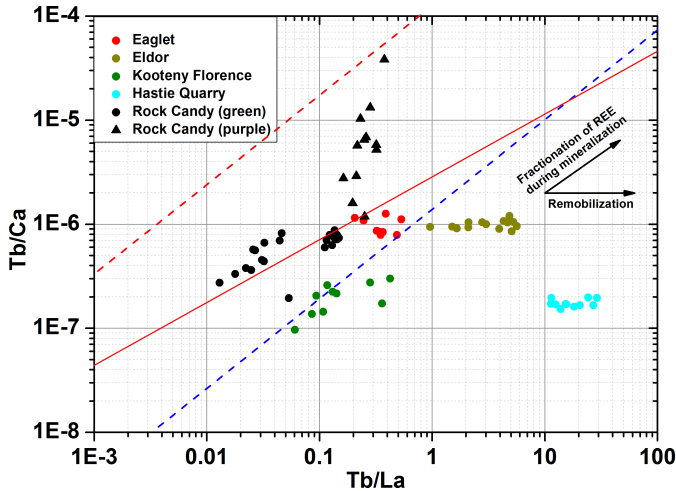


Fig. 4. Tb/La vs. Tb/Ca scatterplot of fluorite from different deposits. The Ca content for all trace-element analyses is assumed to correspond to the stoichiometric composition of ideal fluorite. The red and blue dashed lines are those from Makin et al. (2014). They were recalculated from the Möller (1976) diagram based on atomic proportions of elements rather than their concentrations in ppm. These lines represent the boundaries between fluorite of ‘pegmatitic’, ‘hydrothermal’, and ‘sedimentary’ origins.

the sedimentary field on the Tb/Ca vs. Tb/La diagram (Fig. 4) and shows little variation in Tb/Ca, which is characteristic of a remobilization trend. This phenomenon may be related to the precipitation of LREE-rich mineral phase. At Eldor, monazite is the main ore mineral (Gagnon et al., 2012), which can incorporate most of LREE and leads to La depletion in fluorite (Bau and Dulski, 1995). To better understand the relationships between deposit types and trace element concentrations and behaviors in fluorite, more analyses from different carbonatite samples are required.

4.2. Comparison of LA-ICP-MS(IG) and LA-ICP-MS(FB)

We compare LA-ICP-MS(IG) and LA-ICP-MS(FB) using Sr, Y, and the lanthanides, which are detectable in most fluorite grains (Table 3), and evaluate the relationships between the two methods using X-Y scatter diagrams (Figs. 5-10). Linear regressions for each element were determined using the following equation (from Simandl et al., 2014):

$$[\text{mean value of LA-ICP-MS(IG) result}] = m [\text{LA-ICP-MS(FB) result}] + b$$

Fitted parameters are listed in Table 3. On an X-Y plot, a perfect match between data of the two methods will form a regression line with a slope of unity ($m=1$); the line will pass through the origin (intercept, $b=0$); and the coefficient of determination will equal 1 ($R^2=1$; i.e., all data points plot on the regression line).

In the case of Sr, the best-fit line between the two methods (Fig. 5) is characterized by $m=1.07$, and $R^2=0.995$. This near-perfect fit excludes sample Eaglet9, which has the mean value of Sr determined by LA-ICP-MS(IG) significantly less than the result from the fused bead (Fig. 5; Table 3). The large deviation of the Eaglet9 data from the best-fit line may be due to celestite

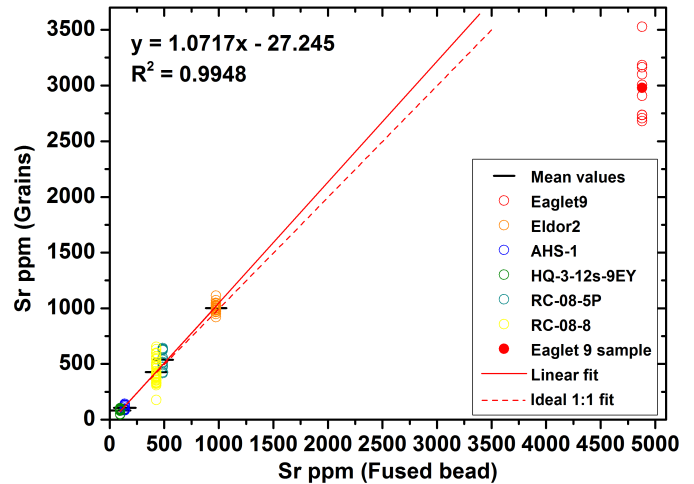


Fig. 5. Comparison of LA-ICP-MS analyses obtained from fused fluorite powder and mean values of individual grains for Sr. Red solid and dashed lines represent fitted regression lines and ideal 1:1 fit, respectively. The red point represents the data which is not used for fitting the regression line.

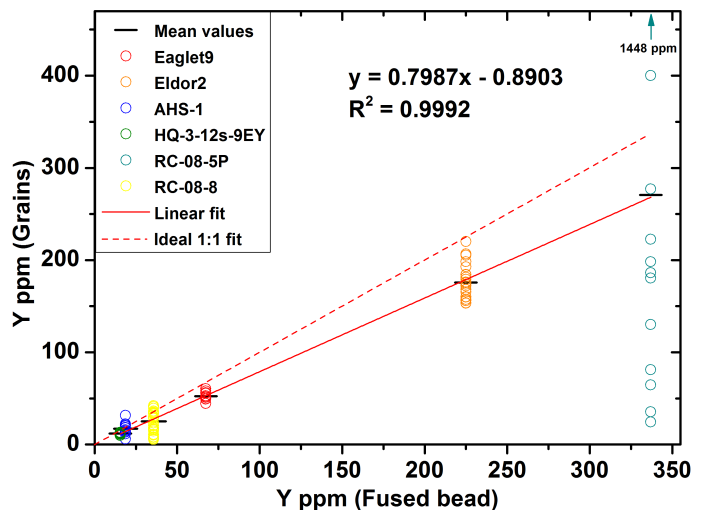


Fig. 6. Comparison of LA-ICP-MS analyses obtained from fused fluorite powder and mean values of individual grains for Y. Red solid and dashed lines represent fitted regression lines and ideal 1:1 fit, respectively.

inclusion(s) or intergrowth with fluorite. Celestite is commonly associated with fluorite at Eaglet (Pell, 1992). This explanation is further supported by the high Ba content (59 ppm) of Eaglet9 from fused bead relative to a mean of 12 analyses at 0.03 ppm from grains (Table 3). Celestite (SrSO_4) and barite (BaSO_4) are end-members of the same solid-solution series.

The sample RC-08-5P (Rock Candy, purple fluorite) shows the highest mean values of all Y and lanthanides relative to other samples (Figs. 6-10; Table 3) but it also has the largest ranges of variations in these elements (Figs. 6-10). This suggests that the fluorite in sample RC-08-5P formed from fluid(s) with highly variable concentrations of these elements (Mauthner and Melanson, 2006). Overall, the results of the

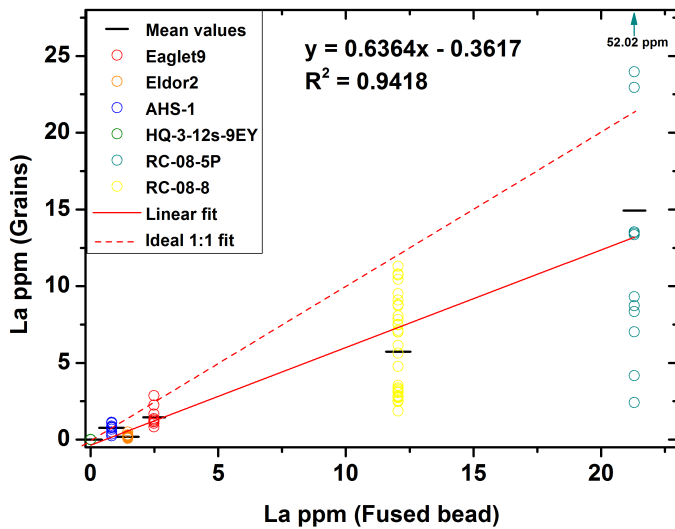


Fig. 7. Comparison of LA-ICP-MS analyses obtained from fused fluorite powder and mean values of individual grains for La. Red solid and dashed lines represent fitted regression lines and ideal 1:1 fit, respectively.

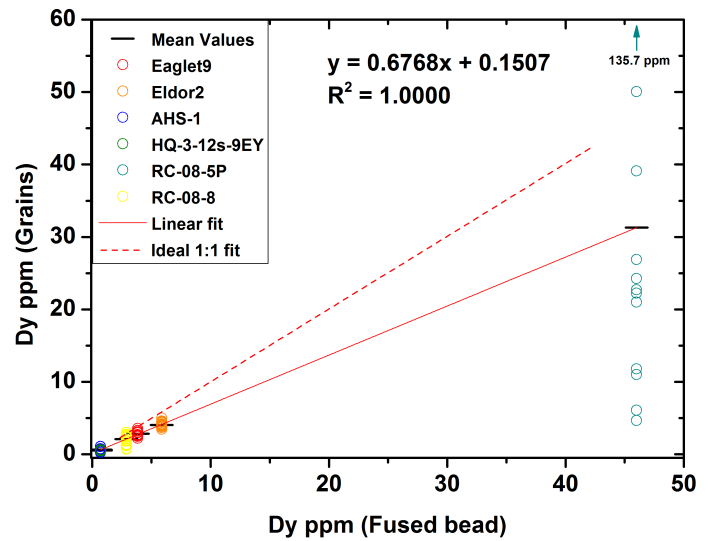


Fig. 9. Comparison of LA-ICP-MS analyses obtained from fused fluorite powder and mean values of individual grains for Dy. Red solid and dashed lines represent fitted regression lines and ideal 1:1 fit, respectively.

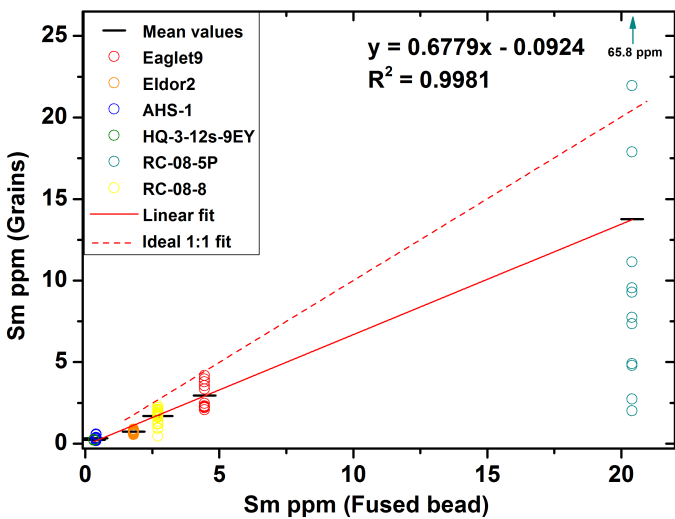


Fig. 8. Comparison of LA-ICP-MS analyses obtained from fused fluorite powder and mean values of individual grains for Sm. Red solid and dashed lines represent fitted regression lines and ideal 1:1 fit, respectively.

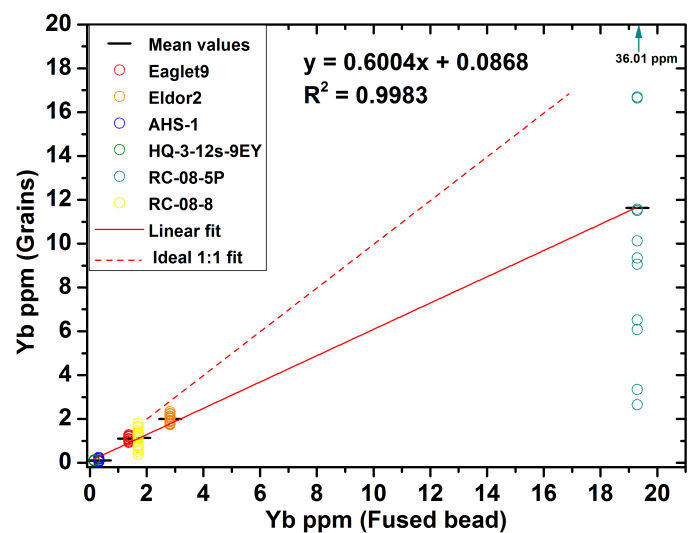


Fig. 10. Comparison of LA-ICP-MS analyses obtained from fused fluorite powder and mean values of individual grains for Yb. Red solid and dashed lines represent fitted regression lines and ideal 1:1 fit, respectively.

lanthanides and Y from fused beads are all notably higher than mean values of results from grains (Figs. 6-10; Table 3). The slope of the fitted regression lines are between 0.60 and 0.68 for the lanthanides, and 0.80 for Y, but the coefficients of determination are between 0.991 and 1.000 for all elements except La (0.94) and Ce (0.98) suggesting consistent differences of trace element contents determined from the two methods (Table 3). The difference between results from the two methods may be caused by the use of different internal standards or the presence of sub-microscopic or microscopic inclusions with elevated-REE abundances.

The differences of lanthanide and Y contents from both laboratories may be caused by the different internal standards

and/or laser sources, which have different fractionation indices for the lanthanides and Y. To determine the content of any trace element, LA-ICP-MS requires that the external standard, internal standard, and sensitivity of the instrument to the detected element must be established. In practice, the selection of these standards depends on the mineral and the elements analyzed (Jackson, 2008). In the LA-ICP-MS(IG) analyses of fluorite, NIST glass was used as the external standard, Ca was the internal standard, and the sensitivities of all elements were determined from NIST glass 611, 613, and 615. However, in LA-ICP-MS(FB) analyses, an internal calibration and standardization process, developed by Bureau Veritas Mineral

Laboratories, was used without external standard. Different laser sources [Nd: YAG 213 nm for LA-ICPMS(IG) and Excimer 193 nm for LA-ICPMS(FB)] can generate distinct fractionation indices that contribute to the difference in results from the two laboratories as previously reported by Gonzalez et al. (2002).

To avoid visible inclusions with elevated-REE, fluorite fragments were screened with a binocular microscope. Furthermore, if an unexpected signal from a potential invisible inclusion was detected during LA-ICP-MS(IG) analyses, the analysis was rejected. However, for the LA-ICP-MS(FB), fluorite and potential tiny inclusions such as monazite and allanite were ground together and incorporated into glass beads. The presence of such sub-microscopic inclusions could cause significant bias. High Zn concentrations (50-175 ppm) measured by LA-ICP-MS(FB) relative to LA-ICP-MS(IG) (<3 ppm) remain unexplained.

5. Summary

Previous studies (Möller et al., 1976; Eppinger and Closs, 1990; Gagnon et al., 2003; Schwinn and Markl, 2005; Makin et al., 2014) and preliminary data analyses in our study all show that fluorite is a potential indicator mineral for deposits such as MVT, carbonatite-related REE, fluorite-barite veins, and peralkaline-related REE deposits. This preliminary study indicates that Sr, Y, and lanthanides in fluorite are quantifiable by LA-ICP-MS(IG). Other elements, such as Mn, Ba, and Th also have potential to discriminate fluorite from different deposit types.

The differences in concentrations between LA-ICP-MS(IG) and LA-ICP-MS(FB) points to dangers of comparing results acquired using different instrumentation, methodology and data reduction. LA-ICP-MS(IG) has an advantage over LA-ICP-MS(FB) for indicator mineral studies, because smaller samples (single grain) are required, whereas many grains are required to create a single fused bead. The negative effects of mineral inclusions on data quality of LA-ICP-MS(IG) can be easily avoided by discarding data with anomalous spectra. The variations in chemical composition of fluorite grains from individual deposits suggest that ideally at least five fluorite grains per sample are required to discriminate deposit types.

Acknowledgments

This project was funded by the Targeted Geoscience Initiative 4 (TGI4), a Natural Resources Canada programme carried out under the auspices of the Geological Survey of Canada in collaboration with the British Columbia Geological Survey. Suggestions and constructive comments by John Carter of Bureau Veritas Mineral Laboratories, Perth are greatly appreciated.

References cited

Alvin, M.P., Dunphy, J.M., and Groves, D.I., 2004. Nature and genesis of a carbonatite-associated fluorite deposit at Speewah, East Kimberley region, Western Australia. *Mineralogy and Petrology*, 80, 127-153.

- Andrade, F.R.D., Möller, P., Lüders, V., Dulski, P., and Gilg, H.A., 1999. Hydrothermal rare earth elements mineralization in the Barra do Itapirapuã carbonatite, southern Brazil: behaviour of selected trace elements and stable isotopes (C,O). *Chemical Geology*, 155, 91-113.
- Bailey, A.D., Hunt, R.P., and Taylor, K.N.R., 1974. An ESR study of natural fluorite containing manganese impurities. *Mineralogical Magazine*, 39, 705-708.
- Bau, M., and Dulski, P., 1995. Comparative study of yttrium and rare-earth element behaviours in fluorine-rich hydrothermal fluids. *Contributions to Mineralogy and Petrology*, 199, 213-223.
- Bau, M., Romer, R.L., Lüders, V., and Dulski, P., 2003. Tracing element sources of hydrothermal mineral deposits: REE and Y distribution and Sr-Nd-Pb isotopes in fluorite from MVT deposits in the Pennine Orefield, England. *Mineralium Deposita*, 38, 992-1008.
- Baxter, J.W., Bradbury, J.C., and Hester, N.C., 1973. A Geologic Excursion to Fluorspar Mines in Hardin and Pope Counties, Illinois. Illinois State Geological Survey, Guidebook Series II, 28p.
- Berry, L.G., Mason, B., and Dietrich, R.V., 1983. *Mineralogy, Concepts, Descriptions, Determinations*. San Francisco, W.F. Freeman, 561p.
- Bettencourt, J.S., Leite Jr., W.B., Goraieb, C.L., Sparrenberger, I., Bello, R.M.S., and Payolla, B.L., 2005. Sn-polymetallic greisen-type deposits associated with late-stage rapakivi granites, Brazil: fluid inclusion and stable isotope characteristics. *Lithos*, 80, 363-386.
- Bill, H., and Calas, G., 1978. Color centers, associated rare-earth ions and the origin of coloration in natural fluorites. *Physics and Chemistry of Minerals*, 3, 117-131.
- Borrok, D.M., Kesler, S.E., Boer, R.H., and Essene, E.J., 1998. The Vergenoeg Magnetite-Fluorite Deposit, South Africa: Support for a Hydrothermal Model for Massive Iron Oxide Deposits. *Economic Geology*, 93, 564-586.
- Bosce, S., and Rakovan, J., 2002. Surface-structure-controlled sectoral zoning of the rare earth elements in fluorite from Long Lake, New York, and Bingham, New Mexico, U.S.A. *Geochimica et Cosmochimica Acta*, 66 (6), 997-1009.
- British Columbia Geological Survey MINFILE: No. 082ESE070. <http://minfile.gov.bc.ca/report.aspx?f=PDF&r=Minfile_Detail.rpt&minfilno=082ESE070>. Accessed on 6th Oct. 2015.
- British Columbia Geological Survey MINFILE: No. 082FNE016. <http://minfile.gov.bc.ca/report.aspx?f=PDF&r=Minfile_Detail.rpt&minfilno=082FNE016>. Accessed on 6th Oct. 2015.
- Bureau Veritas Mineral Laboratories, 2015. LX001 package description. Bureau Veritas Mineral Laboratories, internal unpublished document, Perth, Australia, p.1.
- Cardellach, E., Canal, A., and Grandia, F., 2002. Recurrent hydrothermal activity induced by successive extensional episodes: the case of the Berta F-(Pb-Zn) vein system (NE Spain). *Ore Geology Reviews*, 22, 133-144.
- Cheetham, A., Fender, B., and Cooper, M., 1971. Defect structure of calcium fluoride containing excess anions: I. Bragg scattering. *Journal of Physics C: Solid State Physics*, 4, 3107-3121.
- Chesley, J.T., Halliday, A.N., Kyser, T.K., and Spry, P.G., 1994. Direct dating of Mississippi Valley-type mineralization: Use of Sm-Nd in fluorite. *Economic Geology*, 89, 1192-1199.
- Cunningham, C.G., Rasmussen, J.D., Steven, T.A., Rye, R.O., Rowley, P.D., Romberger, S.B., and Selverstone, J., 1998. Hydrothermal uranium deposits containing molybdenum and fluorite in the Marysvale volcanic field, west-central Utah. *Mineralium Deposita*, 33, 477-494.
- Deer, W.A., Howie, R.A., and Zussman, J., 1965. *Rock-forming minerals*. Halsted Press, London, 347-353.
- Deng, X., Chen, Y., Yao, J., Bagas, L., and Tang, H., 2014. Fluorite REE-Y (REY) geochemistry of the ca. 850 Ma Tumen molybdenite-fluorite deposit, eastern Qinling, China: Constraints

- on ore genesis. *Ore Geology Reviews*, 63, 532-543.
- Eppinger, R.G., and Closs, L.G., 1990. Variation of trace elements and rare earth elements in fluorite: A possible tool for exploration. *Economic Geology*, 85, 1896-1907.
- Fourie, P.J., 2000. The Vergenoeg fayalite Fe-oxide fluorite deposit, South Africa: some new aspects. In: Porter, T.M. (Eds.), *Hydrothermal Fe-oxide copper-gold and related deposits: a global perspective*. Australian Mineral Foundation, Adelaide, pp. 309-320.
- Fulton III, R.B., and Miller, M.M., 2006. Fluorspar. In: Kogel, J.E. et al (Eds.), *Industrial Minerals and Rocks*, 7th Edition. Society for Mining Metallurgy and Exploration, Inc., pp. 461-473.
- Fyles, J.T., 1967. *Geology of the Ainsworth-Kaslo area*, British Columbia. British Columbia Geological Survey Bulletins, 53.
- Gagnon, J.E., Samson, I.M., Fryer, B.J., and Williams-Jones, A.E., 2003. Compositional heterogeneity in fluorite and the genesis of fluorite deposits: Insights from LA-ICP-MS analysis. *The Canadian Mineralogist*, 41, 365-382.
- Gagnon, G., Rousseau, G., Camus, Y., and Gagné, J., 2012. NI 43-101 Technical Report, Preliminary Economic Assessment: Ashram rare earth deposit for Commerce Resources Corporation. <http://www.commerceresources.com/assets/docs/reports/2015-01-07_GG-PEA-Report.pdf> Accessed on 12th Sep. 2015.
- Gonzalez, J., Mao, X.L., Roy, J., Mao, S.S., and Russo, R.E., 2002. Comparison of 193, 213 and 266 nm laser ablation ICP-MS. *Journal of Analytical Atomic Spectrometry*, 17, 1108-1113.
- González-Partida, E., Carrillo-Chávez, A., Grimmer, J.O.W., Pironon, J., Mutterer, J., and Levresse, G., 2003. Fluorite deposits at Encantada-Buenavista, Mexico: products of Mississippi Valley type process. *Ore Geology Reviews*, 23, 107-124.
- Grogan, R.M., and Bradbury, J.C., 1967. Origin of the stratiform fluorite deposits of southern Illinois. *Economic Geology Monograph*, 3, 40-51.
- Grogan, R.M., and Bradbury, J.C., 1968. Fluorite-zinc-lead deposits of the Illinois-Kentucky mining district. In: Ridge, J.D., (eds.), *Ore deposits of the United States, 1933-1967*: New York. American Institute of Mining, Metallurgy, and Petroleum Engineers, pp. 370-399.
- Grogan, R.M., and Montgomery, G., 1975. Fluorspar and Cryolite. In: Lefond, S.J., (Eds.), *Industrial Minerals and Rocks*, 4th Edition, New York. American Institute of Mining, Metallurgical, and Petroleum Engineers Inc., pp. 653-677.
- Hagni, R.D., 1999. Mineralogy of beneficiation problems involving fluorspar concentrates from carbonatite-related fluorspar deposits. *Mineralogy and Petrology*, 67, 33-44.
- Hill, G.T., Campbell, A.R., and Kyle, P.R., 2000. Geochemistry of the southwestern New Mexico fluorite occurrences, implications for precious metals exploration in fluorite-bearing systems. *Journal of Geochemical Exploration*, 68, 1-20.
- Hora, Z.D., Langrova, A., and Pivec, E., 2008. Eaglet property revisited: fluorite-molybdenite porphyry-like hydrothermal system, east-central British Columbia (NTS 093A/10W). *Geological Fieldwork 2007*, British Columbia Geological Survey, 17-30.
- Jackson, S.E., 2008. Calibration strategies for elemental analysis by LA-ICP-MS. In: Sylvester, P. (Eds.), *Laser Ablation-ICP-MS in the Earth Sciences current practices and outstanding issues*. Mineralogical Association of Canada Short Course 40, Vancouver, B.C., pp. 169-188.
- Jochum, K.P., Weis, U., Stoll, B., Kuzmin, D., Yang, Q., Raczek, I., Jacob, D.E., Stracke, A., Birbaum, K., Frick, D.A., Günther, D., and Enzweiler, J., 2011. Determination of Reference Values for NIST SRM 610-617 Glasses Following ISO Guidelines. *Geostandards and Geoanalytical Research*, 35, 397-429.
- Kesler, S.E., Gesink, J.A., and Haynes, F.M., 1989. Evolution of mineralizing brines in the east Tennessee Mississippi Valley-type ore fields. *Geology*, 17, 466-469.
- Kogut, A.I., Hagni, R.D., and Schneider, G.I.C., 1998. *Geology, mineralogy, and paragenetic sequence of the Okorusu carbonatite-related fluorite ores, Namibia*. In: Schweizerbart'sche, E. (Eds.), *Proceedings of the Quadrennial IAGOD Symposium*, 9, pp. 555-573.
- Levresse, G., Trittle, J., Villareal, J., and González-Partida, E., 2006. The "El Pilote" fluorite skarn: A crucial deposit in the understanding and interpretation of the origin and mobilization of F from northern Mexico deposits. *Journal of Geochemical Exploration*, 89, 205-209.
- Lu, H.-Z., Liu, Y., Wang, C., Xu, Y., and Li, H., 2003. Mineralization and fluid inclusion study of the Shizhuyuan W-Sn-Bi-Mo-F skarn deposit, Hunan Province, China. *Economic Geology*, 98, 955-974.
- Makin, S.A., Simandl, G.J., and Marshall, D., 2014. Fluorite and its potential as an indicator mineral for carbonatite-related rare earth element deposits. In: *Geological Fieldwork 2013*, British Columbia Ministry of Energy and Mines, British Columbia Geological Survey Paper 2014-1, 207-212.
- Mauthner, M., and Melanson, F., 2006. Fluorite occurrences in Canada. *Rocks & Minerals*, 81, 114-120.
- Min, M., Fang, C., and Fayek, M., 2005. Petrography and genetic history of coffinite and uraninite from the Liueyiqi granite-hosted uranium deposit, SE China. *Ore Geology Reviews*, 26, 187-197.
- Misra, K.C., and Lu, C., 1992. Hydrothermal calcites from the Mississippi Valley-type Elmwood-Gordonsville zinc deposits, Central Tennessee, U.S.A.: Fluid inclusion and stable isotope data. *European Journal of Mineralogy*, 4, 977-988.
- Mortensen, J.K., Montgomery, J.R., and Phillipone, J., 1987. U-Pb zircon, monazite, and sphene ages for granitic orthogneiss of the Barkerville Terrane, east-central British Columbia. *Canadian Journal of Earth Sciences*, 24, 1261-1266.
- Möller, P., Parekh, P.P., and Schneider, H.-J., 1976. The application of Tb/Ca-Tb/La abundance ratios to problems of fluorspar genesis. *Mineralium Deposita*, 11, 111-116.
- Munoz, M., Preno, W.R., and Vourjault-Radé, 2005. Sm-Nd dating of the fluorite from the Montroc fluorite deposit, southern Massif Central, France. *Mineralium Deposita*, 39, 970-975.
- Pelch, M.A., Appold, M.S., Emsbo, P., and Bodnar, R.J., 2015. Constraints from fluid inclusion compositions on the origin of Mississippi Valley-Type mineralization in the Illinois-Kentucky district. *Economic Geology*, 110, 787-808.
- Pell, J., 1992. Fluorspar and fluorine in British Columbia. *British Columbia Geological Survey*, Open file 1992-16.
- Richardson, C.K., and Pinckney, D.M., 1984. The chemical and thermal evolution of the fluids in the Cave-in-Rock fluorspar district, Illinois: Mineralogy, paragenesis and fluid inclusions. *Economic Geology*, 79, 1833-1856.
- Ruiz, J., Kesler, S.E., Jones, L.M., and Sutter, J.L., 1980. *Geology and geochemistry of the Las Cuevas fluorite deposit, San Luis Potosi, Mexico*. *Economic Geology*, 75, 1200-1209.
- Salvi, S., and Williams-Jones, A.E., 2006. Alteration, HFSE mineralization and hydrocarbon formation in peralkaline igneous systems: Insights from Strange Lake Pluton, Canada. *Lithos*, 90, 19-24.
- Schwinn, G., and Markl, G., 2005. REE systematics in hydrothermal fluorite. *Chemical Geology*, 216, 225-248.
- Sheppard, R.A., and Mumpton, F. A., 1984. Sedimentary fluorite in a lacustrine zeolitic tuff of the Gila Conglomerate Near Buckhorn, Grant County, New Mexico; *Journal of Sedimentary Research*, 54, 853-860.
- Simandl, G.J., 2009. World fluorspar resources, market and deposit examples from British Columbia, Canada. *British Columbia Geological Survey, Information Circular*, 2009-4, 16 pages.
- Simandl, G.J., Fajber, R., and Paradis, S., 2014. Portable X-ray fluorescence in the assessment of rare earth element-enriched sedimentary phosphate deposits. *Geochemistry: Exploration, Environment, Analysis*, 14, 161-169.
- Staebler, G., Deville, J., Verbeek, E., Richards, R.P., and Cesbron,

- F., 2006. Fluorite: From ancient treasures to modern labs and collections. In: Fisher, J., Jarnot, M., Neumeier, G., Pasto, A., Staebler, G., and Wilson, T. (Eds.), *Fluorite - the collector's choice*. Lithographie, LLC, Connecticut, U.S.A. pp. 4-12.
- Sverdrup, T.L., 1968. Yttrifluorite-yttrocerite-cerfluorite in Norwegian pegmatites. *Contributions to the Mineralogy of Norway*, 37, 245-252.
- Verbeek, E., 2006. Fluorite Luminescence. In: Fisher, J., Jarnot, M., Neumeier, G., Pasto, A., Staebler, G., and Wilson, T. (Eds.), *Fluorite - the collector's choice*. Lithographie, LLC, Connecticut, U.S.A., pp. 13-19.
- Wright, W.R., Mariano, A.N., and Hagni, R.G., 1998. Pyrochlore, mineralization, and glimmerite formation in the Eldor (Lake LeMoynes) carbonatite complex, Labrador Trough, Quebec, Canada. In: *Proceedings of the 33rd Forum on the Geology of Industrial Minerals*. Canadian Institute of Mining, Metallurgy and Petroleum; Special Volume, 50, 205-213.
- Xu, C., Taylor, R.N., Li, W., Kynicky, J., Chakhmouradian, A.R., and Song, W., 2012. Comparison of fluorite geochemistry from REE deposits in the Panxi region and Bayan Obo, China. *Journal of Asian Earth Sciences*, 57, 76-89.
- Xu, C., Zhang, H., Huang, Z., Liu, C., Qi, L., Li, W., and Guan, T., 2004. Genesis of the carbonatite-syenite complex and REE deposit at Maoniuping, Sichuan Province, China: Evidence from Pb isotope geochemistry. *Geochemical Journal*, 38, 67-76.